

• Original Paper •

Characteristics of Mesoscale Convective Systems and Their Impact on Heavy Rainfall in Indonesia's New Capital City, Nusantara, in March 2022

Eddy HERMAWAN¹, Risyanto RISYANTO¹, Anis PURWANINGSIH¹, Dian Nur RATRI^{2,3},
Ainur RIDHO⁴, Teguh HARJANA¹, Dita Fatria ANDARINI^{1,5},
Haries SATYAWARDHANA¹, and Akas Pinarangan SUJALU⁶

¹Research Center for Climate and Atmosphere (PRIMA), National Research and
Innovation Agency (BRIN), Jakarta 10340, Indonesia

²Indonesia Meteorological, Climatological, and Geophysical Agency (BMKG), Jakarta 10720, Indonesia

³Meteorology and Air Quality Group, Wageningen University and Research (WUR),
Droevendaalsesteeg, 6708 Wageningen, The Netherlands

⁴Department of Meteorology, University of Reading, Reading RG6 6ET, United Kingdom

⁵School of Geography, Earth and Atmospheric Sciences, The University of Melbourne, Parkville, Victoria 3010, Australia

⁶Department of Agrotechnology, Faculty of Agriculture, Universitas 17 Agustus 1945 Samarinda,
Samarinda 75123, Indonesia

(Received 20 March 2024; revised 4 June 2024; accepted 24 June 2024)

ABSTRACT

Nusantara, the new capital city of Indonesia, and its surrounding areas experienced intense heavy rainfall on 15–16 March 2022, leading to devastating and widespread flooding. However, the factors triggering such intense heavy rainfall and the underlying physical mechanisms are still not fully understood. Using high-resolution GSMaP (Global Satellite Mapping of Precipitation) data, we show that a mesoscale convective system (MCS) was the primary cause of the heavy rainfall event. The rainfall peak occurred during the MCS's mature stage at 1800 UTC 15 March 2022, and diminished as it entered the dissipation stage. To understand the large-scale environmental factors affecting the MCS event, we analyzed contributions from the MJO, equatorial waves, and low-frequency variability to column water vapor and moisture flux convergence. Results indicate a substantial influence of the MJO and equatorial waves on lower-level (boundary layer) meridional moisture flux convergence during the pre-MCS stage and initiation, with their contributions accounting for up to 80% during the growth phase. Moreover, while La Niña and the Asian monsoon had negligible impacts on MCS moisture supply, we find a large contribution from the residual term of the water vapour budget during the maturation and decay phases of the MCS. This suggests that local forcing (such as small-scale convection, local evaporation, land-surface feedback, and topography) also contributed to modulation of the intensity and duration of the MCS. The results of this study can help in our understanding of the potential causes of extreme rainfall in Nusantara and could be leveraged to improve rainstorm forecasting and risk management across the region in the future.

Key words: Nusantara, heavy rainfall, MCS, equatorial waves, low-frequency variability, local effects

Citation: Hermawan, E., and Coauthors, 2025: Characteristics of mesoscale convective systems and their impact on heavy rainfall in Indonesia's new capital city, Nusantara, in March 2022. *Adv. Atmos. Sci.*, **42**(2), 342–356, <https://doi.org/10.1007/s00376-024-4102-1>.

Article Highlights:

- A mesoscale convective system (MCS) was the main driver of heavy rainfall over Nusantara, Indonesia's new capital city, on 15–16 March 2022.
- The MJO and equatorial waves favoured early-stage MCS development, and contributed up to approximately 80% during the growth phase.
- Local forcings such as land-surface feedbacks and topography were likely the main contributors during the maturation and decay phases.
- La Niña and the Asian monsoon had negligible impacts on MCS moisture supply.

* Corresponding authors: Eddy HERMAWAN, Ainur RIDHO
Emails: eddy.hermawan@brin.go.id, a.ridho@student.reading.ac.uk

1. Introduction

Indonesia's new capital, Nusantara, is located in East Kalimantan Province on the east coast of Borneo Island, Indonesia. The city has an equatorial-type climate, characterized by hot, humid, and rainy conditions throughout the year. Rainfall is more frequent and intense from December to March, and there is a noticeable decrease from June to October. This pattern is indicative of a semi-typical monsoonal (bimodal) pattern, where the year is divided into periods of lower and higher rainfall intensities. The driest months span from June to August, while the wettest are from December to February.

On 15–16 March 2022, Nusantara and its surrounding areas—including central, south, north, and west Balikpapan as well as Balikpapan City—experienced intense heavy rainfall, leading to devastating and widespread flooding. According to the Regional Disaster Management Agency, this flood event, triggered by heavy rainfall that began at 0300 local time, affected 2837 households and approximately 9000 individuals (Supriatin, 2022). Additionally, a subsequent landslide, induced by the heavy rains and unstable soil conditions, impacted 31 families. The disaster also had significant effects on housing, with floodwaters reaching levels between 40 and 150 cm in Balikpapan (Muhari, 2022). Despite these significant socioeconomic impacts, the factors triggering such intense heavy rainfall and the underlying physical mechanisms are still not fully understood. Understanding the drivers behind this heavy rainfall is crucial for developing future mitigation strategies.

In the tropics, intense rainfall often results from organized clusters of large cumulonimbus clouds or thunderstorms, known as mesoscale systems (MCSs), which can significantly endanger lives and damage property (Chen et al., 2023; Bao et al., 2024). MCSs are organized assemblages of thunderstorms that produce distinct circulations and features at a larger scale than any individual convective cell (Zipser, 1982). These systems are effective rain producers and important drivers of energy redistribution in the atmosphere (Fritsch and Forbes, 2001). MCSs, which can evolve into tropical cyclones, form along areas where there are tropical waves or easterly waves, which progress westward along monsoon troughs and the Intertropical Convergence Zone in regions of ample low-level moisture, convergent surface winds, and divergent winds aloft (e.g. Latos et al., 2021; Lubis et al., 2022). A recent study has shown that enhanced lower-free-tropospheric moisture, a warmer middle troposphere, and stronger low-level ascent significantly impact the precipitation produced by MCSs in tropical oceans (Chen et al., 2023). An understanding of the mechanisms that cause heavy rainfall related to MCSs over Nusantara in the province of East Kalimantan (including the case in March 2022) is still lacking (Purwaningsih et al., 2022; Marzuki et al., 2023; Ramadhan et al., 2024). This is because of the complexity of the dynamics of the atmosphere over the equator. There is also a lack of discussion about the characteristics of the MCS associated with the heavy rainfall

over Nusantara that happened on 15–16 March 2022. Recently, it was also mentioned by Zhang et al. (2024) that extreme precipitation in Borneo is influenced by the phases of El Niño and La Niña, with sea surface temperature anomalies in the equatorial Pacific affecting these patterns. Borneo experiences extreme precipitation from late December to mid-January and weaker precipitation in February, highlighting the importance of low-frequency climate variability on extreme rainfall in Borneo.

Convectively coupled equatorial waves (CCEWs) are atmospheric disturbances that propagate near the equator, characterized by alternating areas of enhanced and suppressed convection (Wheeler and Kiladis, 1999; Kiladis et al., 2009; Lubis and Jacobi, 2015; Lubis and Respati, 2021). These waves play a crucial role in tropical meteorology, influencing phenomena such as tropical cyclones and the Madden-Julian Oscillation (MJO). These waves have a profound impact on the development and behaviour of organized clusters of thunderstorms or MCSs. CCEWs contribute to the initiation and modulation of MCSs by providing favorable conditions for convection (Latos et al., 2021; Lubis et al., 2022; Cheng et al., 2023). These waves can induce upward motion in the atmosphere, leading to the development of deep convection that organizes into an MCS. Additionally, CCEWs can influence the intensity and spatial distribution of MCSs, affecting their size, duration, and precipitation patterns. In Indonesia, the occurrence of MCSs is closely connected to convective activities over mountainous areas. The intensity of precipitation associated with these systems tends to increase notably when they interact with equatorial Kelvin waves, particularly noticeable for the larger islands such as Sumatra or Borneo (Latos et al., 2021). Moreover, the heavy rainfall experienced in Jakarta, Java, during early January 2020 was also linked to an MCS (Lubis et al., 2022). Therefore, understanding the interactions between CCEWs and MCSs is essential for improving our ability to predict and to better understand the cause of intense heavy rainfall.

In this study, we aim to address the following two key questions:

- What physical process was underlying the occurrence of intense precipitation in Nusantara, during 15–16 March 2022? Specifically, was this event driven by an organized deep convective systems such as an MCS?
- What are the characteristics of MCSs that induce intense rainfall over this area, and what are the environmental conditions conducive to their formation and development?

We will address the first question by focusing on the influence of large-scale atmospheric drivers in creating favourable conditions for the formation and maintenance of the MCS. The characteristics of the MCS-driven heavy rainfall will be examined by using hourly precipitation data from GSMaP (Global Satellite Mapping of Precipitation) and hourly brightness temperature (BT) data from the Himawari-8 satellite. The data and methods that are employed for this study are described in detail in section 2. The results are presented in section 3. Finally, a summary and discussion are provided in section 4.

2. Data and methods

2.1. Dataset

The study area is located on Borneo Island (6° – 5° S, 107.5° – 119.5° E); it focuses on the Penajam Paser Utara region, East Kalimantan, which will become Indonesia's new capital city, Nusantara (Fig. 1). Several types of data were used for the analysis in this study, and they are listed below; the data period is 15–16 March 2022.

In this study, we use the Himawari-8 satellite's BT of infrared channels at $10.4\ \mu\text{m}$ (band 13) to identify the development of convective clouds. Himawari-8 satellite data were taken from the Himawari Cast receiver operated by the National Research and Innovation Agency that is installed in Bandung, West Java, Indonesia. The satellite data used have a $4 \times 4\ \text{km}$ spatial resolution and an hourly temporal resolution. Note that Himawari-8 is a geostationary satellite that covers the Asia-Pacific region, including Indonesia, which is equipped with an Advanced Himawari Imager (AHI) sensor (Da, 2015; Chen et al., 2019b). This AHI sensor makes observations every 10 min and has a 1–2 km spatial grid resolution (Bessho et al., 2016). This relatively high-specification AHI can identify the dynamics and growth of MCSs (Chen et al., 2019a); this is useful for monitoring the potency of heavy rainfall, which can cause disasters such as floods and landslides (Paski et al., 2021).

In addition, the GSMaP gauge-corrected version-7 standard precipitation data product (Zhou et al., 2020) was also used in this study. The GSMaP data are used to analyze the precipitation distribution spatially and temporally; these data were obtained from the Japan Aerospace Exploration Agency's Earth Observation Research Center website (<https://sharaku.eorc.jaxa.jp/GSMaP>). GSMaP is a gridded precipitation product that provides global hourly temporal data with a 0.1° spatial resolution (Ushio et al., 2009). The standard gauge-corrected data are retrieved from a combination of multi-band passive microwave and infrared radiometers adjusted by NOAA/CPC gauge measurements.

ERA5 (fifth major global reanalysis produced by ECMWF) data are also employed in this study. The ERA5

data were obtained from the Copernicus Climate Data Store (<https://cds.climate.copernicus.eu/>). The ERA5 hourly data on pressure levels are used to derive the vertical wind velocity at 925 hPa, the specific humidity, and the horizontal wind velocity (u and v components) at all pressure levels to calculate the vertically integrated water vapour transport (IVT). The data have 37 pressure levels with a $0.25^{\circ} \times 0.25^{\circ}$ spatial resolution and an hourly temporal resolution (Hersbach et al., 2020). The reanalysis data combine models and observations collected from all regions of the world, which makes this dataset a globally complete and consistent dataset that applies to many climate and weather studies. The ERA5 data were also used as the input data for moisture tracking. ERA5 is one of the datasets that provide relatively complex/various parameters needed for transport analysis and understanding the underlying processes, with relatively fine vertical and horizontal resolution. Some limitations could be found in ERA5 data use; for example, the performance of precipitation data is lower than satellite-retrieved data. However, all precipitation datasets, including both ERA5 and satellite data, have bias over mountainous areas, which may affect the representation of convective events (Sharifi et al., 2019). Furthermore, several papers have also reported that ERA5 can be used for analyzing convective events by examining the difference between natural and forced convective activity and analyzing extreme rainfall in response to synoptic-scale weather (Latos et al., 2021; Latos et al., 2023; Satiadi et al., 2023; Trismidianto et al., 2023). Moreover, transport analysis using these data has been conducted in several studies (Lubis and Respati, 2021; Hermawan et al., 2022; Purwaningsih et al., 2022), in which they have helped to explain the influence of large-scale circulation on MCS formation over a certain area.

2.2. Methods

In this study, MCSs were identified by using the Grab'em Tag'em Graph'em (GTG) algorithm developed by Whitehall et al (2015). The GTG algorithm has been used in previous studies to analyze MCSs capable of producing heavy precipitation and that led to flooding in Indonesia (Nuryanto et al., 2019; Hermawan et al., 2022; Purwaningsih et al.,

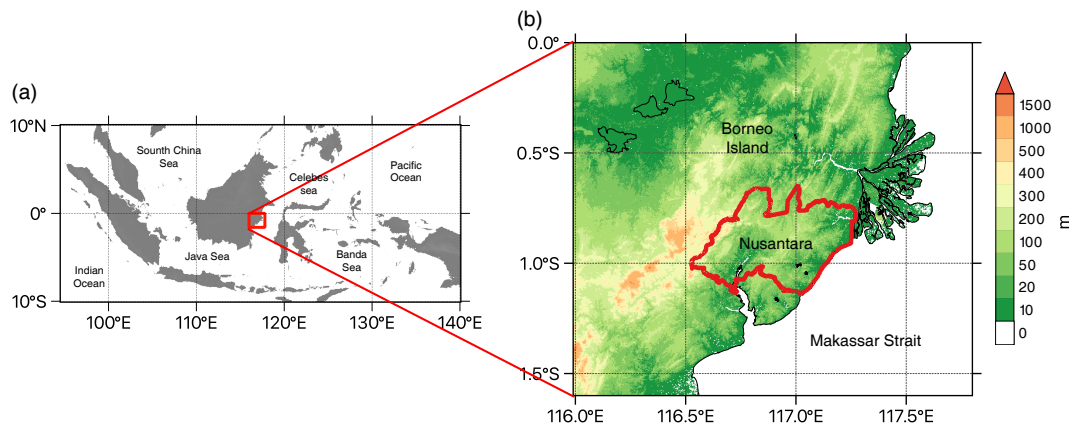


Fig. 1. The (a) study area (red square), located in the middle of the Maritime Continent on the eastern half of Borneo Island, and (b) the administrative border of Nusantara (red outline).

2022). The algorithm is capable of monitoring the complex evolution of MCSs since it allows the merging of multiple convective cells in one timeframe simultaneously (Whitehall et al., 2015). An MCS in this study is defined as an area of contiguous pixels with a BT less than 243 K (Morel and Senesi, 2002) and a minimum size of 2400 km² (Vila et al., 2008) or an area with a BT range of at least 10 K. A minimum duration of three consecutive frames (three hours) should be met for these size and temperature criteria.

An illustration of the development of an MCS from the pre-MCS state until dissipation can be seen in Fig. 2.

In this study, we classified MCSs based on the definition of Jirak et al (2003), which considers four types of MCSs, i.e., mesoscale convective complexes (MCCs), persistent elongated convective systems (PECSs), meso-β circular convective systems (MβCCSs), and meso-β elongated convective systems (MβECSs), based on the cold cloud temperature, size, duration, and shape. The additional two MCS types proposed by Yang et al (2015) are the small meso-β circular convective system (SMβCCS) and the small meso-β elongated convective system (SMβECS). The criteria of these different MCS types are listed in Table 1.

In addition to further investigating the atmospheric conditions during the MCS event, we utilized the precipitation rate data from GSMaP, as well as the vertical wind velocity and the IVT and vertically integrated moisture flux convergence (VIMFC) from the ERA5 data. The IVT was calculated

using zonal and meridional winds and the specific humidity according to the following equation (Van Zomeren and Van Delden, 2007; Latos et al., 2021; Lubis and Respati, 2021; Hermawan et al., 2022; Purwaningsih et al., 2022):

$$IVT = \left[\left(\frac{1}{g} \int_b^a (qu) dp \right)^2 + \left(\frac{1}{g} \int_b^a (qv) dp \right)^2 \right]^{1/2}, \quad (1)$$

where g represents the acceleration due to gravity; q is the specific humidity ($g\text{ kg}^{-1}$); p is the pressure (Pa); and u and v represent the zonal and meridional wind velocities, respectively ($m\text{ s}^{-1}$); a is the upper limit of each layer; and b is the bottom layer of each layer. VIMFC, meanwhile, is calculated using the following equation:

$$VIMFC = -\nabla \cdot \left(\int_b^a q \mathbf{V} \frac{dp}{g} \right), \quad (2)$$

where $\nabla(\cdot)$ denotes the divergence of the moisture flux, \int_b^a represents the vertical integration from the surface pressure b to the top of the atmosphere pressure a , q is the specific humidity, \mathbf{V} is the horizontal wind vector, dp is the differential element of pressure, and g is the acceleration due to gravity, which is used to convert the pressure coordinate integration into a mass per unit area. In subsequent analyses, we quantify the VIMFC using the unit of $\times 10^{-5} (kg\text{ m}^{-2}\text{ s}^{-1})$.

In this study, VIMFC is calculated for two distinct air

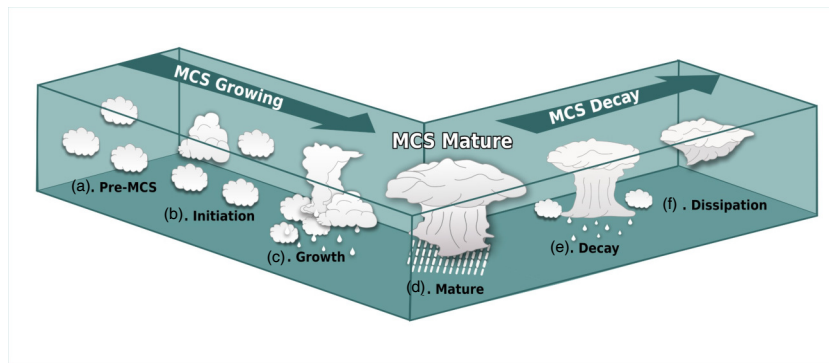


Fig. 2. Illustration of the MCS lifecycle, from pre-formation to initiation, growth, maturity, decay, and final dissipation.

Table 1. MCS classification based on Jirak et al. (2003) and Yang et al. (2015).

MCS Category	Size	Duration	Shape
MCC	Cold cloud region $\leq 221\text{ K}$ with an area $\geq 50\,000\text{ km}^2$	Size definition met for $\geq 6\text{ h}$	Eccentricity ≥ 0.7 at time of maximum extent
PECS			$0.2 \leq$ eccentricity < 0.7 at time of maximum extent
MβCCS	Cold cloud region $\leq 221\text{ K}$ with an area $\geq 30\,000\text{ km}^2$, and maximum size must be $\geq 50\,000\text{ km}^2$	Size definition met for $\geq 3\text{ h}$	Eccentricity ≥ 0.7 at time of maximum extent
MβECS			$0.2 \leq$ eccentricity < 0.7 at time of maximum extent
SMβCCS	Cold cloud region $\leq 221\text{ K}$ with an area $\geq 30\,000\text{ km}^2$, and maximum size must be $\geq 50\,000\text{ km}^2$		Eccentricity ≥ 0.7 at time of maximum extent
SMβECS			$0.2 \leq$ eccentricity < 0.7 at time of maximum extent

columns: first, between 700 and 300 hPa, defined as free-troposphere VIMFC; and second, between 1000 and 850 hPa, referred to as boundary layer VIMFC, which will be illustrated in the following section. If the VIMFC is positive, it indicates that moisture is converging into the column, potentially leading to cloud formation and precipitation if conditions are favourable. Conversely, a negative value suggests moisture divergence, which could be associated with drying conditions (Lubis et al., 2023).

In addition, a two-dimensional Fast Fourier Transform (2D FFT) is applied to isolate tropical intraseasonal disturbances associated with the MJO and Kelvin, mixed Rossby–gravity (MRG), and equatorial waves, enabling clearer differentiation from randomly modulated periodic noise (Wheeler and Kiladis, 1999; Kiladis et al., 2009; Lubis and Jacobi, 2015). The 2D FFT decomposes tropical disturbances in space and time. Symmetric constraints have not been imposed in the filtering process following Lubis and Jacobi (2015).

3. Results

3.1. Heavy rainfall characteristics

Figure 3 shows the average monthly rainfall in Sepaku, a district in Nusantara, using data from rain gauges spanning from 2009 to 2020. The seasonal rainfall variation is consistent with a semi-typical monsoonal pattern, with the region receiving its highest rainfall in December, followed by a secondary peak in April. Conversely, the lowest rainfall is observed in August. There is considerable variation in monthly rainfall over the years, as indicated by the wide standard deviation. This variability can be explained by the geographical location of Nusantara, which lies at the boundary between regions characterized by monsoonal and equatorial rainfall types (Aldrian and Dwi Susanto, 2003; Purwadani et al., 2023).

On 15 and 16 March 2022, Nusantara and its surrounding areas experienced an extended period of intense rainfall, lasting from 1400 to 000 UTC. The peak intensity, recorded at 1800 UTC, reached 17 mm h, as depicted in Fig. 4a. Subsequently, the rainfall intensity gradually decreased until 0200 UTC 16 March. The cumulative rainfall from 0600 UTC 15

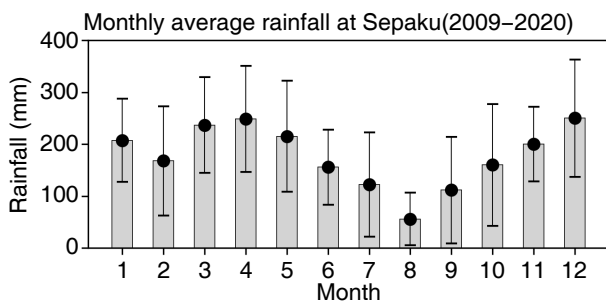


Fig. 3. Monthly average rainfall in Sepaku for the period of 2009 to 2020, with error bars (depicted as vertical black lines) indicating the standard deviation for each respective month.

March to 0600 UTC 16 March reached 101.8 mm, thus qualifying as a very heavy rainfall event according to the criteria set by Meteorological, Climatological, and Geophysical Agency (BMKG) (which is defined by exceeding 100 mm within a 24-hour timeframe). Figure 4b shows the precipitation accumulation and the average 850-hPa wind pattern during this period. It reveals that heavy rainfall was widespread, particularly in the southern inland and offshore areas of Nusantara. Additionally, the 850-hPa wind pattern indicates Nusantara as a convergence zone for westerly and northeasterly winds, favouring the occurrence of intense precipitation. Although not all of Nusantara area received over 100 mm of precipitation, the inner area, specifically the Sepaku District, did indeed experience very heavy rainfall.

3.2. MCS-induced heavy rainfall

To investigate whether the heavy rainfall event over Nusantara was triggered and modulated by an MCS, this section examines the MCS lifecycle using the BT of the 10.4 μm infrared channel from Himawari-8 satellite data. Figure 5 illustrates the evolution of the MCS lifecycle, represented by each of the six MCS stages overlaid with the precipitation rate from GSMaP and the ERA5 horizontal wind at 850 hPa. Overall, the MCS formed and existed for about 12 hours, from 1200 UTC 15 March 2022 (initiation stage) to 0000 UTC 16 March 2022 (dissipation stage). This duration is considered a short-lived MCS, persisting for less than 14

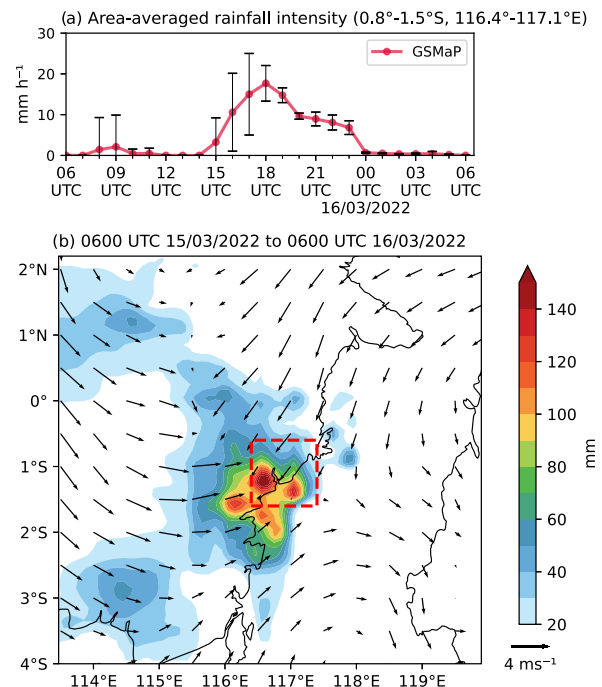


Fig. 4. (a) Area-averaged hourly precipitation for Nusantara and the surrounding areas, based on GSMaP data from 0600 UTC 15 March to 0600 UTC 16 March 2022; (b) Spatial distribution of rainfall accumulation (colour shading) and 850-hPa horizontal winds (vectors) from 0600 UTC 15 March to 0600 UTC 16 March 2022, in Nusantara and the surrounding region. The red dashed frame indicates the boundary used to calculate the area-averaged hourly precipitation.

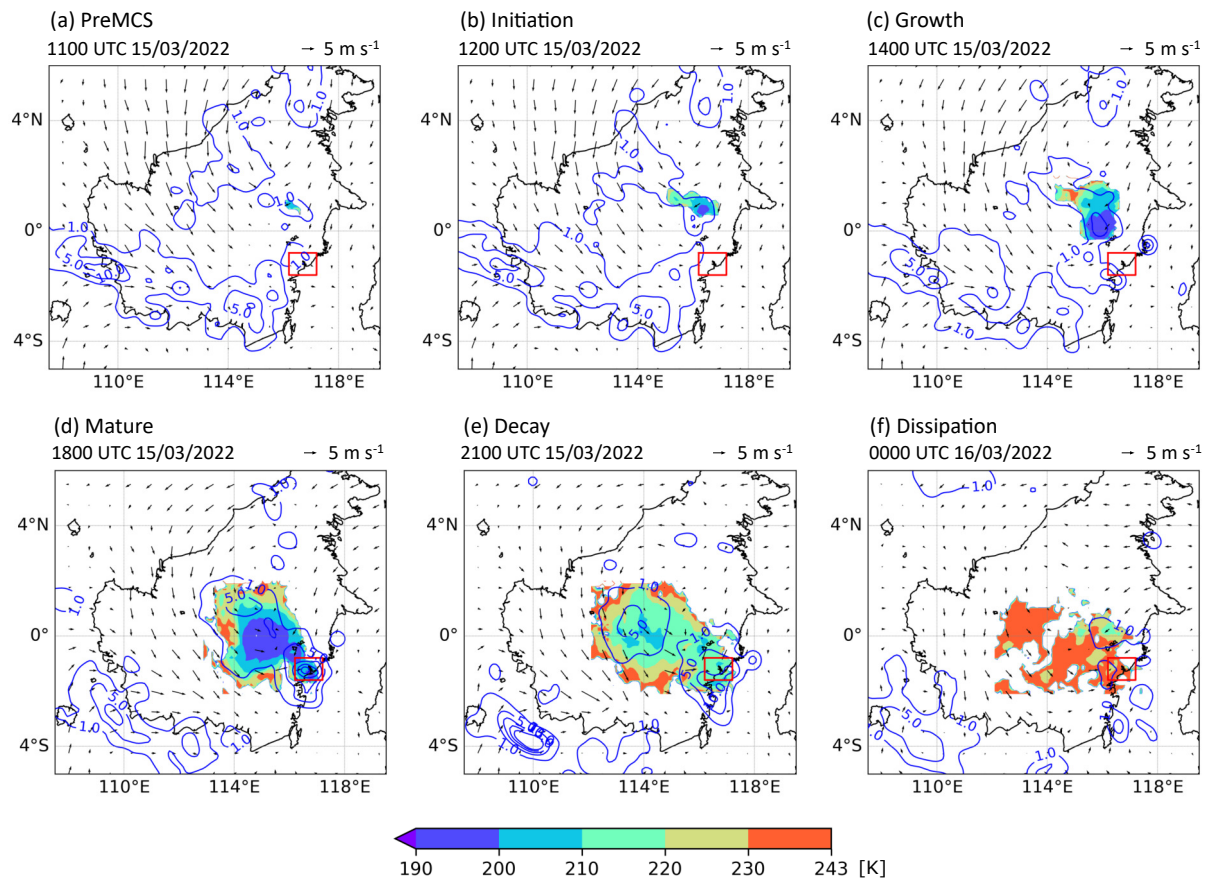


Fig. 5. Brightness temperature ($10.4 \mu\text{m}$) from the Himawari-8 satellite (colour-shaded; units: K) superimposed on GSMaP precipitation rates (contours; units: mm h^{-1}) and 850-hPa wind (vectors; units: m s^{-1}), which can be used to distinguish each MCS stage: (a) pre-MCS stage at 1100 UTC 15 March 2022; (b) initiation stage at 1200 UTC 15 March 2022; (c) growth stage at 1400 UTC 15 March 2022; (d) mature stage at 1800 UTC 15 March 2022; (e) decay stage at 2100 UTC 15 March 2022; and (f) dissipation stage at 0000 UTC 16 March 2022. The location of Indonesia's new capital city, Nusantara, is marked by the red box.

hours, as commonly occurs in Indonesia (Putri et al., 2017).

Initially, during the pre-MCS stage, a small cloud cluster emerged in the northern area of Indonesia's new capital city, Nusantara, covering about 2416 km^2 (Fig. 5a). This cloud cluster continued to develop during the initiation stage, expanding to $13\,968 \text{ km}^2$ (Fig. 5b). The cloud cluster further enlarged to $39\,904 \text{ km}^2$ during the growth stage, which began at 1400 UTC and lasted for four hours (Fig. 5c). The MCS reached its mature stage at 1800 UTC (Fig. 5d), with the cloud area expanding to $120\,000 \text{ km}^2$ and the average BT dropping to 215.4 K . The altitude of this minimum BT distribution is estimated to be around 14–16 km (Hamada and Nishi, 2010). At this stage, the center of the cloud clusters shifted slightly toward the center of Borneo Island, enveloping the Nusantara area. At the same time, the maximum rainfall observed from the GSMaP data at Nusantara aligns the timing of the mature MCS stage with the peak in rainfall. The mature stage persisted for three hours before the MCS began to decay at 2100 UTC (Fig. 5e). During the decay stage, the cloud area increased to $164\,576 \text{ km}^2$, exceeding that of the mature stage; however, the average BT rose to 222.5 K , indicating a decrease in cloud-top height. The

MCS lifecycle concluded in the dissipation stage at 0000 UTC (Fig. 5f), marked by a warmer cloud temperature and a reduction in the area of cold clouds ($\text{BT} \leq 221 \text{ K}$).

The properties of the MCS, including the cloud area, temperature, eccentricity, and type for each stage, are presented in Table 2. Generally, the MCS exhibited a circular shape with an eccentricity greater than 0.7, except during the initiation stage, when its eccentricity was 0.67. In the mature stage, the MCS could be classified as an MCC, featuring an eccentricity of 0.92 and meeting the size criteria for six hours. Subsequently, the MCC evolved into a circular shape and was classified as an M β CCS, with an eccentricity of 0.84. This shape remained relatively unchanged until the MCC dissipated.

The spatial distribution of MCS-induced rainfall rates from GSMaP (color shading) superimposed on the IVT (vector) and the vertical wind velocity (contour) is presented in Fig. 6. In general, the spatial distribution of the rainfall was consistent with the development of the MCS, indicating that the gradual increase (decrease) in rainfall occurred before (after) the MCS's mature stage. The Nusantara area experienced light rainfall ($2\text{--}6 \text{ mm h}^{-1}$) during the pre-MCS

Table 2. Properties of the MCS at each stage calculated by the GTG method.

MCS Stage	BT \leq 243 K Area (km ²)	BT \leq 221 K Area (km ²)	BT Average (K)	Eccentricity	Type
Pre-MCS	2416	1589	217.3	0.89	–
Initiation	13 968	9696	215.6	0.67	–
Growth	39 904	28 160	213.5	0.88	–
Mature	120 000	73 760	215.4	0.92	MCC
Decay	164 576	87 712	222.5	0.84	M β CCS
Dissipation	119 040	5440	234.8	0.72	–

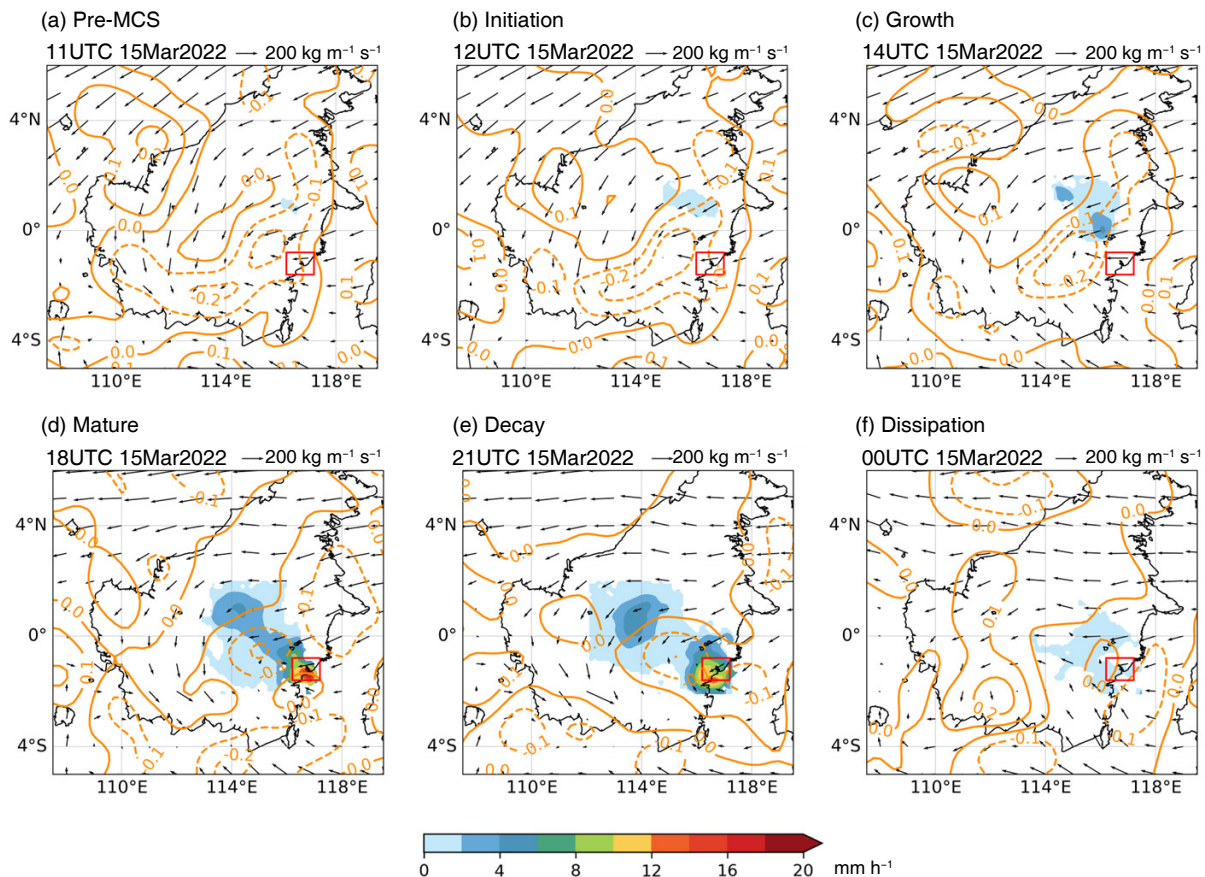


Fig. 6. GSMaP precipitation driven by the MCS (colour-shaded; units: mm h⁻¹) superimposed with the IVT (vectors; units: kg m s⁻¹) and vertical wind velocity (contours; units: Pa s⁻¹) for each MCS stage: (a) pre-MCS stage at 1100 UTC 15 March 2022; (b) initiation stage at 1200 UTC 15 March 2022; (c) growth stage at 1400 UTC 15 March 2022; (d) mature stage at 1800 UTC 15 March 2022; (e) decay stage at 2100 UTC 15 March 2022; and (f) dissipation stage at 0000 UTC 16 March 2022. The location of Indonesia's new capital city, Nusantara, is marked by the red box.

(Fig. 6a), initiation (Fig. 6b), and growth stages (Fig. 6c). The rainfall reached its maximum during the MCS's mature stage at 1800 UTC 15 March 2022 (Fig. 6d), suggesting that the MCS was the main driver of heavy rainfall over Nusantara. The rainfall consistently decreased during the decay stage (Fig. 6e) and vanished when the MCS was in the dissipation stage (Fig. 6f).

Furthermore, it is also shown that during the lifecycle of MCS-induced heavy rainfall, the sources of moisture over the Nusantara area predominantly came from the northeast from the initial MCS stage until the dissipation stage, as indicated by the vector of IVT (Fig. 6). Some moisture was contributed by sources from the southwest of the Nusan-

tara area, specifically during the MCS's mature and decay stages (Figs. 6d and e). The movement of the vertically integrated water vapor was consistent with the cloud formation shown in Figs. 5a–c; the clouds initially developed in the northern area and expanded to the western area of Nusantara (the centre of Borneo Island). The eastward and westward water vapor transport caused moisture to accumulate in Nusantara, supporting MCS formation and heavy rainfall over this area, as we discuss later in the next section.

3.3. Large-scale environmental factors driving the MCS

3.3.1. Moistening and lifting

To better understand the environmental factors contribut-

ing to the development and evolution of the MCS over the Nusantara area, we first evaluate the characteristics of air moistening and lifting during the MCS cycle. Figure 7 presents an hourly time series of specific humidity at 850 hPa and wind vertical velocity at 500 hPa for several hours before (pre-MCS, initiation, and growth) and after (decay and dissipation stage) the mature stage of the MCS. We derived both specific humidity and vertical velocity from the average values at the center point of MCS clouds (± 1 grid of $0.25^\circ \times 0.25^\circ$). We observed that moistening occurred starting from the pre-MCS stage, as indicated by the continuous increase in specific humidity (Fig. 7a) until it reached a maximum during the mature phase of the MCS. Thereafter, moisture gradually decreased during the decay and dissipation stages. Moreover, the air moistening before the rainfall peak was also supported by lifting, indicated by the negative value of the vertical velocity (Fig. 7b). This air-lifting gradually strengthened and reached its peak at the MCS mature stage, then weakened afterward. During the pre-MCS stage (-7 to -6 hours before the mature stage, Fig. 7b), downward motion was detected over the central MCS area and its vicinity. Lifting began in the initiation stage (-6 to -5 hours before the mature stage, Fig. 7b) with relatively weak vertical velocity (a negative value close to 0 Pa s^{-1}). This lifting gradually strengthened during the growth stage (-4 to -3 hours before the mature stage, Fig. 7b) and peaked during the mature stage at more than -1 Pa s^{-1} . After the mature stage, the updrafts weakened. The vertical velocity gradually decreased to around -0.5 Pa s^{-1} during the decay stage ($+3$ to $+4$ hours after the mature

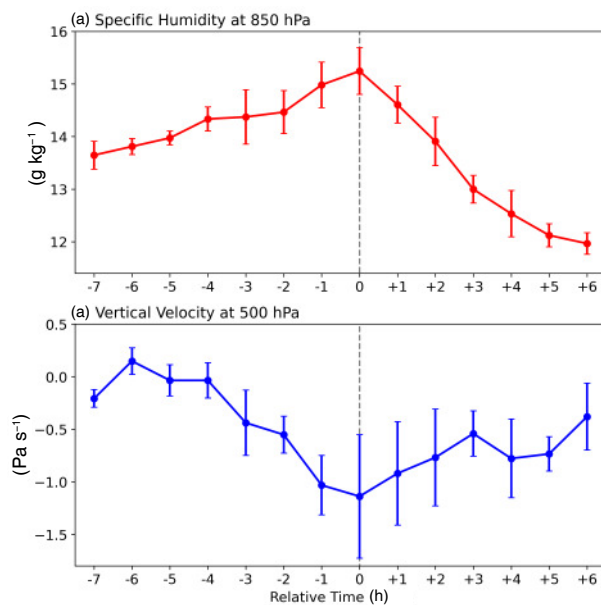


Fig. 7. Time series of (a) specific humidity at 850 hPa (units: g kg^{-1}) and (b) vertical velocity at 500 hPa (units: Pa s^{-1}) at the center of the MCS area before and after the mature stage. The x-axis shows the relative time (hours) of the MCS stage, where $t = 0$ indicates the mature stage. Error bars show the standard deviation within ± 1 grid at the center of the MCS area.

stage, Fig. 7b) and to about -0.4 Pa s^{-1} during the dissipation stage ($+5$ to $+6$ hours after the mature stage, Fig. 7b). The abundant moisture and intensive upward motions present during the MCS mature stage corresponded with the occurrence of the peak of heavy rainfall over the Nusantara area. This finding aligns with a previous study conducted by Chen et al (2023), in which it was found that the moistening of the low-level troposphere, associated with low-level upward motions, is significantly correlated with the MCS lifetime and rainfall rate over tropical ocean regions. It is also known that the formation of an MCS requires the presence of ample moisture, instability, and a lifting mechanism to trigger convection, typically found in the tropics where MCSs are commonly observed (Schumacher and Rasmussen, 2020).

To further investigate the moisture responsible for the moistening and lifting of the MCS, we analyze the 72-hour backward trajectories and specific humidity over different altitudes using the HYSPLIT model technique, as shown in Fig. 8. The Lagrangian moisture tracking indicates three main dominant pathways/directions of moisture propagation toward Nusantara, starting from 72 hours prior to 1800 UTC 15 March 2022 (Fig. 8a). Trajectories toward the surface to 750 m above Nusantara mainly contributed to the air moistening (Fig. 8b). These pathways originally came from the south-west (over the terrestrial area) and then deflected westward and southwestward (over the ocean area) toward Nusantara as 1800 UTC 15 March 2022 approached. An increase in moisture was detected over the ocean area (with a specific humidity of more than 14 g kg^{-1}) several hours before it reached the tracking locations (red rectangle). This result is consistent with the idea that the increasing specific humidity supported MCS development before the maturation stage, as shown in Fig. 7a, and reached its highest at the surrounding area of the flooding location at 1800 UTC, during the mature stage of the MCS (Fig. 7a and Fig. 6d). Secondly, the moisture mixing from the southwest and northeast influenced the moistening air over Nusantara above approximately 1000 m and below 4000 m. A combination of air from these two directions was found at 1000, 1500, 2000, and 3000 m (Fig. 8c). Furthermore, higher altitudes correspond to lower specific humidity, as shown in Fig. 8d. The air at 4000, 5000, and 6000 m over Nusantara had dry-air characteristics (at the level from $0\text{--}2 \text{ g kg}^{-1}$). Southwestward and westward motions were detected at these tracking altitudes. Therefore, we can conclude that pathways from the terrestrial (eastern part of Borneo) and ocean (Makassar Strait) areas surrounding the flooding location are likely to have made a higher contribution to the heavy precipitation that occurred over Nusantara at 1800 UTC 16 March 2022 than the pathways from eastern areas (Sulawesi, Maluku, and the surrounding sea).

3.3.2. Roles of MJO and equatorial waves

Thus far, we have identified the source and behavior of moisture during the MCS lifecycle. In addition, it is also important to examine what drives this moisture. This section explores the impact of large-scale moisture transport, espe-

cially by the MJO and equatorial waves, on the preconditioning and development of the MCS during this intense rainfall event.

Figure 9 shows the filtered total precipitable water vapor (TPWV) based on the frequency of various waves, including equatorial Rossby (ER) waves (Fig. 9a), Kelvin waves (Fig. 9b), MJO (Fig. 9c), MRG waves (Fig. 9d), and low-frequency (LF) waves (Fig. 9e). Positive (negative) values represent the wet (dry) phase of the waves. During the flooding period (denoted by the horizontal dashed lines in Fig. 9), the Kelvin and LF waves were in the negative (dry) phase, which brought negative feedback to the moisture supply,

ply over the flooding location. Moreover, the MJO, ER, and MRG waves exhibited their wet phase, where moisture was highly generated by the wave modulation. More specifically, the eastward propagation of the positive phase of the MJO coincides with the westward-positive-phase of ER and MRG waves over the flooding location during the flooding period (denoted by the cross-section between the horizontal and vertical dashed lines in Figs. 9a and c). The combination of the wet phases of the MJO, ER, and MRG waves indicates positive feedback to the moisture supply, supporting the onset of MCS formation and evolution.

To quantify the contributions of the MJO and various

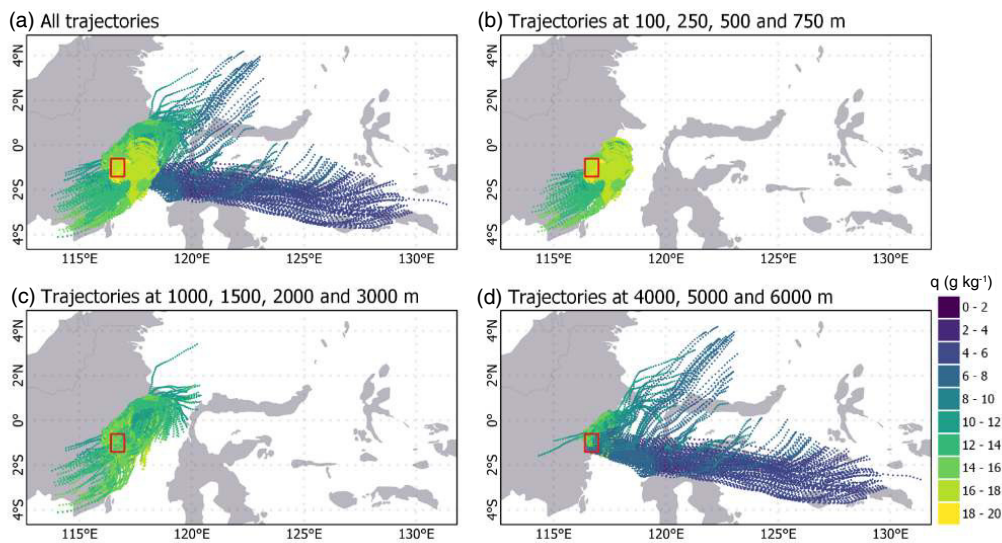


Fig. 8. 72-hour backward trajectories and specific humidity over different altitudes: (a) all trajectories (100 to 6000 m MSL); (b) 100 250 500, and 750 m MSL; (c) 1000, 1500, 2000, and 3000 m MSL; and (d) 4000, 5000, and 6000 m AGL. Moisture tracking was conducted for 1800 UTC 15 March 2022 over 63 points within the red rectangle.

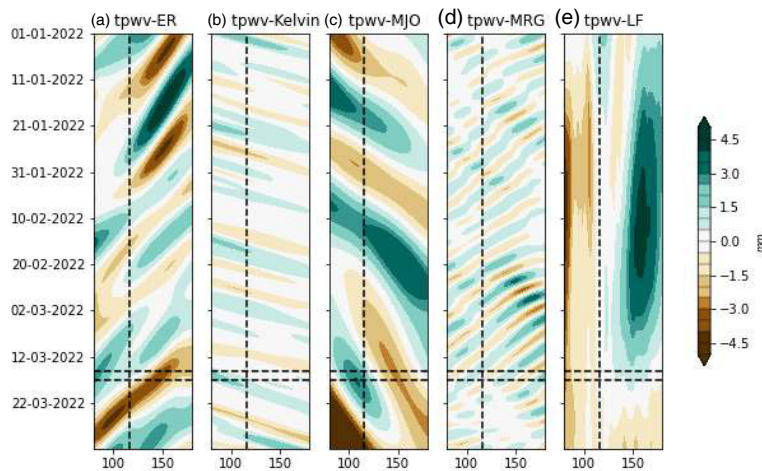


Fig. 9. Hovmöller diagrams of filtered TPWV based on various atmospheric waves: (a) ER waves; (b) Kelvin waves; (c) MJO; (d) MRG waves, and (e) LF disturbances. The vertical dashed lines indicate the longitude of New Capital City, Nusantara, and the horizontal dashed lines indicate the period of heavy rainfall.

types of equatorial waves to the moisture anomaly supporting MCS formation and evolution, we calculate the percentage contributions relative to the total moisture anomaly during the MCS lifecycle (Fig. 10). The total anomaly in Fig. 10a was calculated by subtracting the TPVW from its daily climatology. The percentages are calculated from the ratio between each wave component to the total anomaly. The results show that tropical waves contribute significantly to moisture anomalies, accounting for 173%–231% of the moisture anomaly during the pre-MCS phase and MCS initiation, and 80% during the growth phase of the MCS (Fig. 10a). Specifically, the contributions during the growth phase are primarily driven by equatorial waves (ER and MRG) and the MJO. Furthermore, the contribution of the total waves to the moisture anomaly is lower during the maturation and decay stages as the residual terms dominate, giving rise to the development and decay rate of the MCS. This residual term is likely driven by local factors. This is consistent with previous studies showing that local convergence, local convection, land-surface feedback, or orographic forcing are the local forces that contribute more during these stages (Crook et al., 2023; Galarnau Jr. et al., 2023). Moreover, while the influence of low-frequency variability does positively affect moisture anomalies, it remains weak as the positive phase of La Niña was confined to the eastern part of the Maritime Continent (Fig. 9e). In summary, tropical waves and the MJO modulated the MCS during the early stage (Salahuddin and Curtis, 2009; Maranan et al., 2021), and local forcing took over the role of modulation during the maturation (90%), decay (73%), and dissipation (72%) stages. The roles of local forc-

ing during these stages are believed to have arisen from land-surface feedback mechanisms and topographic influences (Salstein and Rosen, 1994; Hartung et al., 2020). However, further study using numerical weather forecasts and idealized models is needed to quantify and understand the local forcing mechanisms.

Finally, the moisture convergence over the boundary layer and free troposphere is further decomposed based on the filtered waves (Figs. 11a and b). Generally, the contribution of moisture convergence over the boundary layer is more dominant than that in the free troposphere. The dominant contributions of tropical waves (ER and Kelvin) and the MJO during the early stages of the MCS are driven by the lower-level convergence of water vapor (Fig. 11b). The MJO consistently contributes to the moisture convergence during all stages of the MCS, while the ER waves contribute to the moisture convergence only during the early stages. Furthermore, our additional analysis on the meridional and zonal-oriented moisture flux convergence indicated that MCS rainfall over New Capital City—Nusantara could mostly be attributed to the meridional component of VIMFC (not shown). The decomposition of the VIMFC meridional component, based on tropical waves (ER, MRG, and MJO), reveals that the ER waves predominantly contribute to meridional convergence from the Pre-MCS to the growth stage. This contribution is consistent with moisture inflows from the eastern part, as depicted in Fig. 8, reflecting the westward propagation of ER waves. In contrast, this pattern is not observed in the zonal-oriented VIMFC, nor in its decomposition into contributions from different wave types.

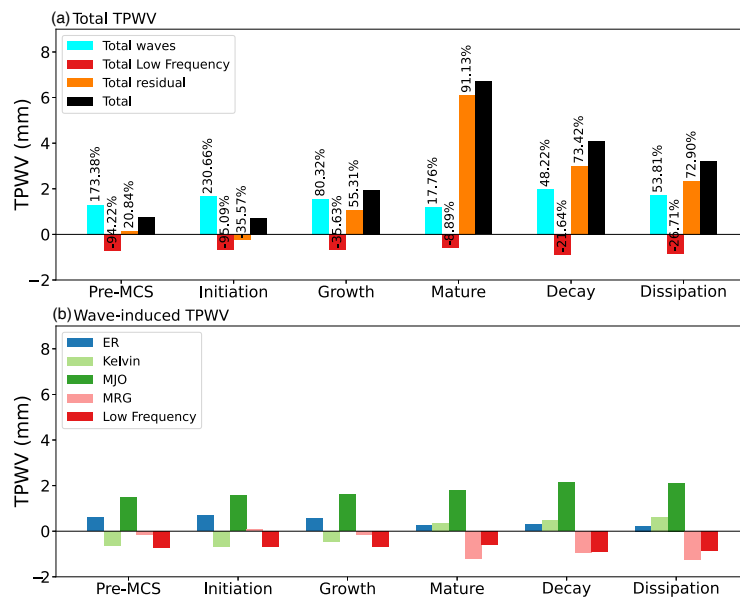


Fig. 10. TPWV budget averaged from the center of the MCS to its vicinity ($\pm 2^\circ$ relative to the center) during various stages of the MCS. The percentage is calculated as the ratio of each filtered-component anomaly with respect to the total anomaly (black bar); (a) Total TPWV: the decomposition of total waves, total LF waves, total residual, and total TPWV; (b) Wave-induced TPWV: the decomposition of ER, Kelvin, MJO, MRG, and LF disturbances.

The MJO's contribution to supporting the MCS in all stages is further discussed based on the MJO index in the next subsection (Fig. 12).

3.3.3. Roles of climate modes of variability

Our results so far demonstrate that the MJO persistently contributed to the moisture sources in all stages of MCS development during the flood incident in Nusantara on 15 March 2022. To further support this evidence, we examine the Hovmöller diagram of the MJO index, along with the Aus-

tralian Monsoon Index (AUSMI), the Indian Ocean Dipole (IOD) index, and the El Niño–Southern Oscillation (ENSO) index (represented by the Niño-3.4 index) from January to early April 2022 (Fig. 12). The Nusantara region is denoted by the vertical black dashed line. It is evident that the Nusantara area experienced several MJO wet phases starting from mid-January with fluctuating amplitudes. Specifically, on 15 March 2022, the wet phase of the MJO signal neared Nusantara, gradually intensified, and persisted for more than 15 days into early April. This suggests that the MJO

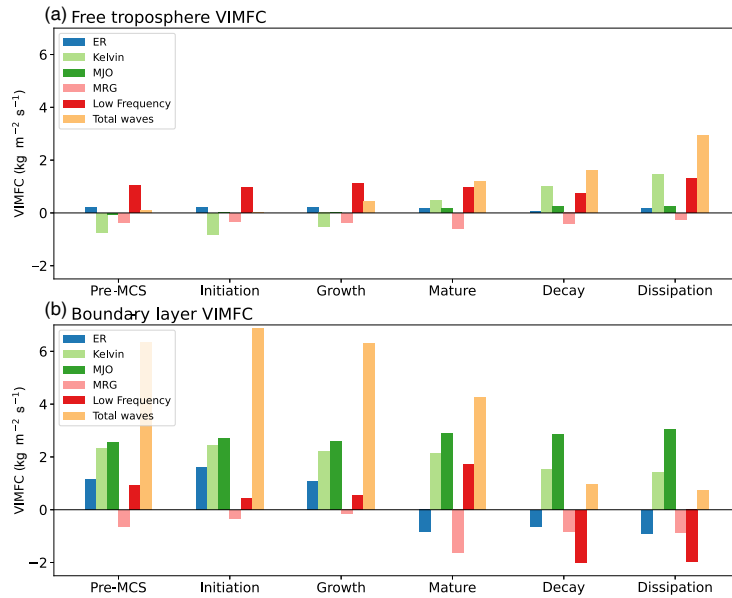


Fig. 11. VIMFC budget at the central MCS and its vicinity ($\pm 2^\circ$ from the center) during various stages of the MCS: (a) free-troposphere VIMFC including ER, Kelvin, MJO, MRG, LF, and total waves; (b) boundary-layer VIMFC including ER, Kelvin, MJO, MRG, LF, and total waves.

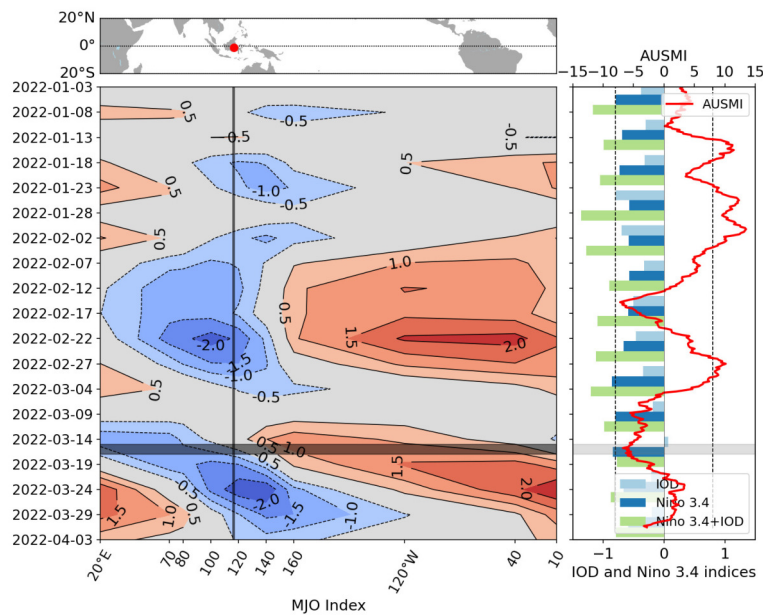


Fig. 12. Time series of the MJO index, AUSMI, IOD index, and Niño-3.4 index indices around the period of intense heavy rainfall in Sepaku on 15 March 2022.

was active during development of the MCS in Nusantara. This aligns with previous findings in Figs. 10 and 11, which illustrated the MJO's continuous contribution to the MCS.

Figure 12 (right-hand panel) also shows the condition of the LF wave signals, including the AUSMI, IOD index, and Niño-3.4 index, during the period from January to April 2022. Generally, the IOD and Niño-3.4 indices exhibit negative values, signifying that the wet phase was active over the Maritime Continent. However, as previously mentioned, we found the influence of LF waves to be negligible, even contributing negatively to the moisture supply associated with formation of the MCS in Nusantara (Fig. 10). Note that the effects of La Niña predominantly affected the eastern region of Indonesia and had not yet impacted the central and western areas of the Maritime Continent, including Nusantara (Supari et al., 2018). Moreover, during the period of heavy rainfall, the AUSMI was in the dry phase, indicating that easterly winds were present and had a negligible impact on the moisture contribution to the MCS. In summary, the climate mode and MJO indices confirm our filtered column water vapour and VMIFC anomalies, showing that the MJO exerted a positive feedback on the moistening environment throughout the MCS cycle. Conversely, low-frequency variability associated with La Niña and the monsoon had only a minimal and negligible impact on the moisture supply for the MCS.

4. Summary and discussion

This study examined the physical processes underlying the intense precipitation events that occurred in Nusantara, the new capital city of Indonesia, on 15–16 March 2022. In particular, our aim was to determine whether these events were driven by organized deep convective systems, such as an MCS. Additionally, we wanted to characterize the MCSs that induce intense rainfall over this area and identify the environmental conditions conducive to their formation and development. By analyzing hourly precipitation data from GSMaP, BT data from the Himawari-8 satellite, ERA5 data, and in-situ observational data, the key findings of our analysis can be summarized as follows:

- An MCS was the main driver of heavy rainfall over Nusantara on 15–16 March 2022. The rainfall reached its maximum during the MCS's mature stage at 1800 UTC 15 March 2022, and then consistently decreased and vanished when the MCS was in the dissipation stage. The abundant moisture and intense upward motions during the MCS mature stage were consistent with the occurrence of the peak of heavy rainfall over the Nusantara area.

- MJO and equatorial waves significantly influenced the early stages of MCS development over the region. Specifically, the MJO and equatorial waves accounted for ~173%–231% of the total moisture (water vapor) anomalies during the pre-MCS stage and the initiation of the MCS, and ~80% during the MCS growth phase. This moisture contribution was primarily driven by the ER and MRG waves, along with the MJO through the lower-level (boundary

layer) moisture flux convergence.

- The residual term in the column water vapor budget predominantly contributed up to ~72%–91% during the mature, decay, and dissipation stages of the MCS. The substantial residual contribution is likely attributable to local factors, which include small-scale convection, local evaporation, land-surface feedbacks, or the influence of topography, especially during the mature and decay phases of the MCS.

- Low-frequency variability, including La Niña and the monsoon system had only a minimal impact on the moisture supply for the MCS.

Given the substantial contribution of the residual term in the mature and dissipation stages of the MCS, it is important to further investigate the role of local processes in MCSs. Previous studies show that such a residual term of the water vapor budget is likely a result of local forcing during these MCS stages, which include small-scale convection, local evaporation, land-surface feedbacks, and/or the influence of topography (Salstein and Rosen, 1994; Hartung et al., 2020). For example, topography could force air to ascend as it flows over mountains or elevated terrain on Borneo Island, leading to adiabatic cooling, condensation, and precipitation (Qian, 2008; Qian et al., 2013). This orographic effect could enhance the intensity and duration of convective systems. Likewise, differential heating of the land surface on Borneo, due to variations in soil moisture, vegetation, and land use, could create areas of low pressure and convergence zones. These conditions, in turn, could increase atmospheric instability and moisture, providing a favorable environment for MCS development. Given the limited scope of our present study, future work will be aimed at testing these hypotheses using numerical weather forecasts and idealized models to deeply explore the role of local forcing mechanisms in MCS development and the associated heavy rainfall. Moreover, additional key synoptic phenomena in Borneo, including the cross-equatorial surge and the Borneo vortex, have the potential to interact with the MJO and MCSs, thereby affecting patterns of extreme precipitation within the region (Liang et al., 2023; Lubis et al., 2023). This aspect will also be explored in future work.

This study emphasizes the importance of MCSs and the combined influence of large-scale and local forcings in triggering heavy rainfall event in Indonesia's new capital city, Nusantara. The insights gained from this study could, therefore, enhance our understanding of the factors contributing to heavy rainfall in Nusantara, which can be leveraged to improve rainstorm forecasting and risk management in the area in the future.

Acknowledgements. We thank Dr. Sandro W. LUBIS from PNNL (Pacific Northwest National Laboratory), USA for his extensive discussions, insightful inputs, and constructive feedback, which were instrumental in the completion of this paper. This research was supported by the Budget Execution (Allotment) Document, National Research and Innovation Agency (BRIN) in 2022 (Grant No. SP DIPA-124.01.1.690504/2022).

Author contributions. EH, R, AP, DNR, AR, TH, and DTA were the main contributors to this manuscript. They drafted the initial manuscript, revised it, improved analysis and discussions of the overall content, and provided simulated data and significant data findings. In addition, others contributed to producing related figures to validate the model from satellite and reanalysis data and produced additional analysis. Finally, all authors agreed to the published version of the manuscript.

Conflicts of interest. The authors declare no conflicts of interest.

Open Access This article is licensed under a Creative Commons Attribution 4.0 International License, which permits use, sharing, adaptation, distribution and reproduction in any medium or format, as long as you give appropriate credit to the original author(s) and the source, provide a link to the Creative Commons licence, and indicate if changes were made. The images or other third party material in this article are included in the article's Creative Commons licence, unless indicated otherwise in a credit line to the material. If material is not included in the article's Creative Commons licence and your intended use is not permitted by statutory regulation or exceeds the permitted use, you will need to obtain permission directly from the copyright holder. To view a copy of this licence, visit <http://creativecommons.org/licenses/by/4.0/>.

REFERENCES

- Aldrian, E., and R. Dwi Susanto, 2003: Identification of three dominant rainfall regions within Indonesia and their relationship to sea surface temperature. *International Journal of Climatology*, **23**, 1435–1452, <https://doi.org/10.1002/joc.950>.
- Bao, J. W., B. Stevens, L. Kluft, and C. Muller, 2024: Intensification of daily tropical precipitation extremes from more organized convection. *Science Advances*, **10**, ead6801, <https://doi.org/10.1126/sciadv.adj6801>.
- Bessho, K., and Coauthors, 2016: An introduction to Himawari-8/9 —Japan's new-generation geostationary meteorological satellites. *J. Meteor. Soc. Japan*, **94**, 151–183, <https://doi.org/10.2151/jmsj.2016-009>.
- Chen, D. D., and Coauthors, 2019a: Mesoscale convective systems in the Asian monsoon region from advanced Himawari imager: Algorithms and preliminary results. *J. Geophys. Res.: Atmos.*, **124**, 2210–2234, <https://doi.org/10.1029/2018JD029707>.
- Chen, X. C., L. R. Leung, Z. Feng, and Q. Yang, 2023: Environmental controls on MCS lifetime rainfall over tropical oceans. *Geophys. Res. Lett.*, **50**, e2023GL103267, <https://doi.org/10.1029/2023GL103267>.
- Chen, Y. P., K. M. Sun, C. Chen, T. Bai, T. Park, W. L. Wang, R. R. Nemani, and R. B. Myneni, 2019b: Generation and evaluation of LAI and FPAR products from Himawari-8 Advanced Himawari Imager (AHI) data. *Remote Sensing*, **11**, 1517, <https://doi.org/10.3390/rs11131517>.
- Cheng, Y. M., J. Dias, G. Kiladis, Z. Feng, and L. R. Leung, 2023: Mesoscale convective systems modulated by convectively coupled equatorial waves. *Geophys. Res. Lett.*, **50**, e2023GL103335, <https://doi.org/10.1029/2023GL103335>.
- Crook, J., F. Morris, R. Fitzpatrick, S. Peatman, J. Schwendike, T. Stein, C. Birch, and S. Hardy, 2023: Impacts of the MJO and equatorial waves on tracked mesoscale convective systems over Southeast Asia. Preprints, EGU General Assembly 2023, Vienna, Austria, EGU, <https://doi.org/10.5194/egu-sphere-egu23-15259>.
- Da, C., 2015: Preliminary assessment of the Advanced Himawari Imager (AHI) measurement onboard Himawari-8 geostationary satellite. *Remote Sensing Letters*, **6**, 637–646, <https://doi.org/10.1080/2150704X.2015.1066522>.
- Fritsch, J. M., and G. S. Forbes, 2001: Mesoscale convective systems. *Meteor. Monogr.*, **28**(50), 323–358, <https://doi.org/10.1175/0065-9401-28.50.323>.
- Galarneau, T. J. Jr., X. B. Zeng, R. D. Dixon, A. Ouyed, H. Su, and W. J. Cui, 2023: Tropical mesoscale convective system formation environments. *Atmospheric Science Letters*, **24**, e1152, <https://doi.org/10.1002/asl.1152>.
- Hamada, A., and N. Nishi, 2010: Development of a cloud-top height estimation method by geostationary satellite split-window measurements trained with CloudSat data. *J. Appl. Meteorol. Climatol.*, **49**, 2035–2049, <https://doi.org/10.1175/2010JAMC2287.1>.
- Hartung, K., T. G. Shepherd, B. J. Hoskins, J. Methven, and G. Svensson, 2020: Diagnosing topographic forcing in an atmospheric dataset: The case of the North American Cordillera. *Quart. J. Roy. Meteor. Soc.*, **146**, 314–326, <https://doi.org/10.1002/qj.3677>.
- Hermawan, E., and Coauthors, 2022: Large-scale meteorological drivers of the extreme precipitation event and devastating floods of Early-February 2021 in Semarang, Central Java, Indonesia. *Atmosphere*, **13**, 1092, <https://doi.org/10.3390/atmos13071092>.
- Hersbach, H., and Coauthors, 2020: The ERA5 global reanalysis. *Quart. J. Roy. Meteor. Soc.*, **146**, 1999–2049, <https://doi.org/10.1002/qj.3803>.
- Jirak, I. L., W. R. Cotton, and R. L. McAnelly, 2003: Satellite and radar survey of Mesoscale Convective System development. *Mon. Wea. Rev.*, **131**, 2428–2449, [https://doi.org/10.1175/1520-0493\(2003\)131<2428:SARSOM>2.0.CO;2](https://doi.org/10.1175/1520-0493(2003)131<2428:SARSOM>2.0.CO;2).
- Kiladis, G. N., M. C. Wheeler, P. T. Haertel, K. H. Straub, and P. E. Roundy, 2009: Convectively coupled equatorial waves. *Rev. Geophys.*, **47**, RG2003, <https://doi.org/10.1029/2008RG000266>.
- Latos, B., and Coauthors, 2021: Equatorial waves triggering extreme rainfall and floods in southwest Sulawesi, Indonesia. *Mon. Wea. Rev.*, **149**, 1381–1401, <https://doi.org/10.1175/MWR-D-20-0262.1>.
- Latos, B., and Coauthors, 2023: The role of tropical waves in the genesis of Tropical Cyclone Seroja in the Maritime Continent. *Nature Communication*, **14**, 856, <https://doi.org/10.1038/s41467-023-36498-w>.
- Liang, J., J. L. Catto, M. K. Hawcroft, L. Tan, K. I. Hodges, and J. M. Haywood, 2023: Borneo Vortices in a warmer climate. *Npj Climate and Atmospheric Science*, **6**, 2, <https://doi.org/10.1038/s41612-023-00326-1>.
- Lubis, S. W., and C. Jacobi, 2015: The modulating influence of convectively coupled equatorial waves (CCEWs) on the variability of tropical precipitation. *International Journal of Climatology*, **35**, 1465–1483, <https://doi.org/10.1002/joc.4069>.
- Lubis, S. W., and M. R. Respati, 2021: Impacts of convectively coupled equatorial waves on rainfall extremes in Java, Indonesia. *International Journal of Climatology*, **41**, 2418–2440, <https://doi.org/10.1002/joc.6967>.
- Lubis, S. W., S. Hagos, C. C. Chang, K. Balaguru, and L. R.

- Leung, 2023: Cross-equatorial surges boost MJO's southward detour over the maritime continent. *Geophys. Res. Lett.*, **50**, e2023GL104770, <https://doi.org/10.1029/2023GL104770>.
- Lubis, S. W., and Coauthors, 2022: Record-breaking precipitation in Indonesia's capital of Jakarta in Early January 2020 linked to the Northerly Surge, Equatorial Waves, and MJO. *Geophys. Res. Lett.*, **49**, e2022GL101513, <https://doi.org/10.1029/2022GL101513>.
- Maranan, M., A. Schlueter, A. H. Fink, and P. Knippertz, 2021: Influence of tropical waves on the lifecycle of mesoscale convective systems over West Africa. Preprints, EGU General Assembly 2021, Online, EGU, <https://doi.org/10.5194/egu-sphere-egu21-10716>.
- Marzuki, M., R. Ramadhan, H. Yusnaini, M. Vonnisa, R. Safitri, and E. Yanfatriani, 2023: Changes in extreme rainfall in new capital of Indonesia (IKN) based on 20 years of GPM-IMERG data. *Trends in Sciences*, **20**, 6935–6935, <https://doi.org/10.48048/tis.2023.6935>.
- Morel, C., and S. Senesi, 2002: A climatology of mesoscale convective systems over Europe using satellite infrared imagery. I: Methodology. *Quart. J. Roy. Meteor. Soc.*, **128**, 1953–1971, <https://doi.org/10.1256/003590002320603485>.
- Muhari, A., 2022: Banjir dan Tanah Longsor Melanda Sejumlah Kecamatan di Kota Balikpapan. Available from <https://bnpb.go.id/berita/banjir-dan-tanah-longsor-melanda-sejumlah-kecamatan-di-kota-balikpapan->.
- Nuryanto, D. E., H. Pawitan, R. Hidayat, and E. Aldrian, 2019: Characteristics of two mesoscale convective systems (MCSs) over the Greater Jakarta: Case of heavy rainfall period 15–18 January 2013. *Geoscience Letters*, **6**, 1, <https://doi.org/10.1186/s40562-019-0131-5>.
- Paski, J. A. I., D. S. Permana, N. Alfuadi, M. F. Handoyo, M. H. Nurrahmat, and E. E. S. Makmur, 2021: A multiscale analysis of the extreme rainfall triggering flood and landslide events over Bengkulu on 27th April 2019. *AIP Conference Proceedings*, **2320**, 040019, <https://doi.org/10.1063/5.0037508>.
- Purwadani, N. N., M. R. Djuwansah, M. R. Abdillah, F. R. Fajary, and I. Narulita, 2023: Extreme rainfall clusters in Borneo and their synoptic climate causes. *Proc. Int. Conf. on Radioscience, Equatorial Atmospheric Science and Environment and Humanosphere Science*. Singapore, Springer, 407–415, https://doi.org/10.1007/978-981-19-9768-6_38.
- Purwaningsih, A., and Coauthors, 2022: Moisture origin and transport for extreme precipitation over Indonesia's New Capital City, Nusantara in August 2021. *Atmosphere*, **13**, 1391, <https://doi.org/10.3390/atmos13091391>.
- Putri, N. S., T. Hayasaka, and K. D. Whitehall, 2017: The properties of mesoscale convective systems in Indonesia detected using the Grab 'Em Tag 'Em Graph 'Em (GTG) algorithm. *J. Meteor. Soc. Japan*, **95**, 391–409, <https://doi.org/10.2151/jmsj.2017-026>.
- Qian, J. H., 2008: Why precipitation is mostly concentrated over islands in the Maritime Continent. *J. Atmos. Sci.*, **65**, 1428–1441, <https://doi.org/10.1175/2007JAS2422.1>.
- Qian, J. H., A. W. Robertson, and V. Moron, 2013: Diurnal cycle in different weather regimes and rainfall variability over Borneo associated with ENSO. *J. Climate*, **26**, 1772–1790, <https://doi.org/10.1175/JCLI-D-12-00178.1>.
- Ramadhan, R., M. Marzuki, W. Suryanto, S. Sholihun, H. Yusnaini, and R. Muharsyah, 2024: Rainfall variability in Indonesia new capital associated with the Madden-Julian Oscillation and its contribution to flood events. *Quaternary Science Advances*, **13**, 100163, <https://doi.org/10.1016/j.qsa.2024.100163>.
- Salahuddin, A., and S. Curtis, 2009: Evolution of mesoscale convective systems and its relationship with the Madden-Julian oscillation in the Indo-Pacific region. *The Open Atmospheric Science Journal*, **3**, 158–171, <https://doi.org/10.2174/1874282300903010158>.
- Salstein, D. A., and R. D. Rosen, 1994: Topographic forcing of the atmosphere and a rapid change in the length of day. *Science*, **264**, 407–409, <https://doi.org/10.1126/science.264.5157.407>.
- Satiadi, D., and Coauthors, 2023: Impacts of CENS and MJO phenomena on diurnal cycle of local convection, moisture convergence, and rainfall over land, coast, and sea areas in the western part of Java Island. *Meteorol. Atmos. Phys.*, **135**, 42, <https://doi.org/10.1007/s00703-023-00979-w>.
- Schumacher, R. S., and K. L. Rasmussen, 2020: The formation, character and changing nature of mesoscale convective systems. *Nature Reviews Earth & Environment*, **1**, 300–314, <https://doi.org/10.1038/s43017-020-0057-7>.
- Sharifi, E., J. Eitzinger, and W. Dorigo, 2019: Performance of the state-of-the-art gridded precipitation products over mountainous terrain: A regional study over Austria. *Remote Sensing*, **11**, 2018, <https://doi.org/10.3390/rs11172018>.
- Supari, F. Tangang, E. Salimun, E. Aldrian, A. Sopaheluwakan, and L. Juneng, 2018: ENSO modulation of seasonal rainfall and extremes in Indonesia. *Climate Dyn.*, **51**, 2559–2580, <https://doi.org/10.1007/s00382-017-4028-8>.
- Supriatin, 2022: Banjir dan Longsor Landa Balikpapan, Lebih dari 9.000 Jiwa Terdampak. Available from <https://www.merdeka.com/peristiwa/banjir-dan-longsor-landa-balikpapan-lebih-dari-9000-jiwa-terdampak.html>.
- Trismidianto, and Coauthors, 2023: Interactions among Cold Surge, Cross-Equatorial Northerly Surge, and Borneo Vortex in influencing extreme rainfall during Madden-Julian oscillation over the Indonesia Maritime Continent. *Meteorol. Atmos. Phys.*, **135**, 43, <https://doi.org/10.1007/s00703-023-00978-x>.
- Ushio, T., and Coauthors, 2009: A Kalman filter approach to the Global Satellite Mapping of Precipitation (GSMaP) from combined passive microwave and infrared radiometric data. *J. Meteor. Soc. Japan*, **87A**, 137–151, <https://doi.org/10.2151/jmsj.87A.137>.
- Van Zomeren, J., and A. Van Delden, 2007: Vertically integrated moisture flux convergence as a predictor of thunderstorms. *Atmospheric Research*, **83**, 435–445, <https://doi.org/10.1016/j.atmosres.2005.08.015>.
- Vila, D. A., L. A. T. Machado, H. Laurent, and I. Velasco, 2008: Forecast and tracking the evolution of cloud clusters (ForTraCC) using satellite infrared imagery: Methodology and validation. *Wea. Forecasting*, **23**, 233–245, <https://doi.org/10.1175/2007WAF2006121.1>.
- Wheeler, M., and G. N. Kiladis, 1999: Convectively coupled equatorial waves: Analysis of clouds and temperature in the wavenumber–frequency domain. *J. Atmos. Sci.*, **56**, 374–399, [https://doi.org/10.1175/1520-0469\(1999\)056<0374:CCEWAO>2.0.CO;2](https://doi.org/10.1175/1520-0469(1999)056<0374:CCEWAO>2.0.CO;2).
- Whitehall, K., and Coauthors, 2015: Exploring a graph theory based algorithm for automated identification and characterization of large mesoscale convective systems in satellite datasets. *Earth Science Informatics*, **8**, 663–675, <https://doi.org/10.1007/s12145-014-0181-3>.

- Yang, X. R., J. F. Fei, X. G. Huang, X. P. Cheng, L. M. V. Carvalho, and H. R. He, 2015: Characteristics of mesoscale convective systems over China and its vicinity using geostationary satellite FY2. *J. Climate*, **28**, 4890–4907, <https://doi.org/10.1175/JCLI-D-14-00491.1>.
- Zhang, W. J., R. G. Wu, P. X. Dai, and S. W. Yeh, 2024: Why does extreme precipitation occur in Borneo during both El Niño and La Niña winters?. *J. Geophys. Res.: Atmos.*, **129**, e2023JD040415, <https://doi.org/10.1029/2023JD040415>.
- Zhou, Z. T., B. Guo, W. X. Xing, J. Zhou, F. L. Xu, and Y. Xu, 2020: Comprehensive evaluation of latest GPM era IMERG and GSMaP precipitation products over mainland China. *Atmospheric Research*, **246**, 105132, <https://doi.org/10.1016/j.atmosres.2020.105132>.
- Zipser, E. J., 1982: Use of a conceptual model of the life-cycle of mesoscale Convective Systems to improve very-short-range forecasts. Available from <https://api.semanticscholar.org/CorpusID:134080695>.